Master's Thesis
석사 학위논문

Preparation of Oxygen Deficient Black Titania for Visible Light Assisted Hydrogen Production

Jong-Pil Jeon (전 종 필, 全 鍾 弼)

Department of Energy Systems Engineering
에너지시스템공학전공

DGIST

2017

Master's Thesis
석사 학위논문

Preparation of Oxygen Deficient Black Titania for Visible Light Assisted Hydrogen Production

Jong-Pil Jeon (전 종 필, 全 鍾 弼)

Department of Energy Systems Engineering
에너지시스템공학전공

DGIST

2017

Preparation of Oxygen Deficient Black Titania for Visible Light Assisted Hydrogen Production

Advisor : Professor Jong-Sung Yu
Co-advisor : Dr. Sang Kyoo Lim

by

Jong-Pil Jeon
Department of Energy Systems Engineering
DGIST

A thesis submitted to the faculty of DGIST in partial fulfillment of the requirements for the degree of Master of Science in the Department of Energy System Engineering. The study was conducted in accordance with Code of Research Ethics[1]

12. 27. 2016

Approved by

Professor Jong-Sung Yu(Signature)
(Advisor)

Dr. Sang Kyoo Lim(Signature)
(Co-Advisor)

---

[1] Declaration of Ethical Conduct in Research: I, as a graduate student of DGIST, hereby declare that I have not committed any acts that may damage the credibility of my research. These include, but are not limited to: falsification, thesis written by someone else, distortion of research findings or plagiarism. I affirm that my thesis contains honest conclusions based on my own careful research under the guidance of my thesis advisor.

Preparation of Oxygen Deficient Black Titania for Visible Light Assisted Hydrogen Production

Jong-Pil Jeon

Accepted in partial fulfillment of the requirements for the degree of
Master of Science.

12. 05. 2016

Head of Committee________________(인)
Prof. Jong-Sung Yu
Committee Member________________(인)
Dr. Sang Kyoo Lim
Committee Member________________(인)
Prof. Jong-Soo Lee

MS/ES
201524011

전 종 필. Jong-Pil Jeon. Preparation of Oxygen Deficient Black Titania for Visible Light Assisted Hydrogen production. Department of Energy Systems Engineering. 2017. 39p. Advisor Prof. Yu, Jong-Sung, Co-Advisor Dr. Lim, Sang Kyu.

Abstract

Black TiO_2 is defects engineered material to enhance optical properties. However, in spite of the remarkable improvement and extent optical absorption to visible light, it is failed to demonstrate expected photocatalytic activity due to the presence of a number of recombination centers. In this report, reduced black TiO_2 is prepared by a new approach which is the controlled magnesiothermic reduction under a 5% H_2/Ar atmosphere. After reduction, surface defects are produced such as oxygen vacancies, surface lattice disorder, and hydrogenation and, as a result, band structure also changed. The prepared material possesses an optimal band structure, surface defects, oxygen vacancies, and charge recombination centers and exhibit dramatically enhanced optical absorption in the visible and infrared region. The combinations induce synergistic effects to make black TiO_2 material possible to show an outstanding hydrogen production ability in the methanol-water system in the presence of Pt as a co-catalyst. The material shows remarkable stability and shows the maximum hydrogen production rates are 43 mmol h^{-1} g^{-1} and 440μmol h^{-1} g^{-1} under the full solar wavelength range of light and visible light, respectively, and these are remarkably enhanced values than previously reported black TiO_2 materials.

Keywords: Photocatalyst, TiO_2, water splitting, band gap, oxygen vacancy

Contents

List of tables

List of figures

I. INTRODUCTION

1.1 Motivation

Most of the energy that we use is gotten from fossil fuels such as petroleum, coal, and natural gas. Even though the energy getting from the fossil fuels accelerated the development of civilization, science, and technology, the indiscriminate uses destroyed environment and induce detrimental effect on the earth such as green-house effect. Not only the environmental disruption but also the finite deposits of fossil fuels arouse the interests to sustainable and eco-friendly energy sources. As alternative clean energy source to substitute fossil fuels, hydrogen has been considered one of the most promising candidates with development of fuel cells technology. With oxygen, hydrogen directly can be converted to energy, from chemical energy to electrical energy, and water in the fuel cells system. Due to the abundance and non-toxicity, the importance of hydrogen is highly increased. Currently, most of the hydrogen is produced from steam reforming of fossil fuels. The produced hydrogen not only have less energy than original fuels, some of it being lost as heat as like a combustion engine, but also induce carbon dioxide emissions during the production. Only about 4% is produced by water electrolysis, which is required quite high cost. As a clean and cheap way, photo-induced hydrogen generation take center stage on research area. A number of results are reported about it such as photoelectrochemical water splitting, photoelectrocatalytic production, and photochemical water splitting. Because solar energy is practically infinite and eco-friendly, photo-induced hydrogen generation is one of ideal methods which are powerful, low cost, and environmental. Since the discovery of Honda and Fujishima[52], numerous photocatalysts have been reported, such as the combination of metals, metal alloys, metal modified with transition metal(TM) phosphides, TM sulphides, and TM oxides. Each of the materials has pros and cons.

Transition metal oxide has been researched a long time. Due to the high stability and semiconducting property, it is commonly researched as a photocatalyst. TiO_2 is one of the presentative and promising metal oxide materials, which utilized in photo induced reaction. It is stable in the presence of light and highly efficient as a photocatalyst. Despite of the superiorities, it has limitation which is only sensitive to light of high energy. TiO_2 only can absorb ultraviolet (UV) light, which occupy only around 4 % in sunlight, due to the wide band-gap.[51] To utilize visible and infrared light, which account for most part of sunlight, several different approaches have been achieved to enhance absorbance capacity and extend absorption region to longer wavelength by band-gap engineering. The approaches mainly related to make defects such as doping of metals and non-metals, and oxygen vacancies. These efforts have enhanced visible light absorption and the photocatalytic activity, but the results are not sufficiently high.

1.2 Precedented researches

Chen et al. reported hydrogenated black TiO_2 with enhanced solar light absorption.[5] The hydrogenated TiO_2 shows significant enhanced visible light absorption and photocatalytic hydrogen production.[6-16] Different groups tried to prepare hydrogenated and reduced TiO_2 with various colors like yellow, blue, gray, and black from different initial TiO_2 materials at different reaction conditions. Lu et al. studied how the color of commercial Degussa P25 change, when employing a high pressure hydrogen (35 bar) environment.[12] Liu et al. reported black TiO_2 nanotube arrays prepared at a high pressure H_2 treatment, with enhanced activity.[13] Sun et al. studied black TiO_2 nanocrystals with different facets prepared at high pressure.[14] Qiu et al. reported blue rutile TiO_2 which was rapidly synthesized under 40 bar pressure at 450°C.[17] Yu et al. prepared hydrogenated anatase TiO_2 nanosheets in the presence of hydrogen gas at

500-700°C by varying the time periods to lead gradual changes in color from blue to gray.[15] Li et al. prepared grey mesoporous anatase TiO_2 microspheres by a hydrogen gas treatment.[18] Wang et al. prepared yellowish green and black hydrogenated rutile TiO_2 nanowire arrays by changing temperature under hydrogen gas.[6] Naldoni et al. prepared black TiO_2 nanoparticles with H_2 stream and amorphous TiO_2 and the effect of the cooling process also studied.[19] Liang et al. reported hydrogenated anatase TiO_2 inverse opal structure, and the material was prepared by hydrogen-argon or nitrogen treatment at high temperature.[20] Danon et al. reported the effect of reactor materials to the properties of reduced TiO_2.[7,10,16,21-24] Hoang et al. prepared reduced TiO_2 nanowire arrays by co-treatment of H_2 and NH_3 and showed the synergistic effect with Ti^{3+}, N, and hydrogenation.[10] Myung et al. prepared black TiO_2 nanoparticles using yellow TiO_2 gel under argon at 400-600°C.[25] To investigate the improvement of optical properties and photocatalytic activity of reduced or hydrogenated TiO_2, several factors were considered such as oxygen vacancies, surface lattice disorders, the presence of Ti^{3+}, Ti-OH and Ti-H groups on the surface, and engineered band structure. However, these factors are not clearly proved how it work exactly, and the results depends on the combination of various factors, mainly depending on the synthetic methods.[11] Later on, several different synthetic methods like hydrogen plasma, chemical reduction, chemical oxidation, and electrochemical reduction have been used to prepare black TiO_2.[11,13,26-37] Besides photocatalysis, black TiO_2 is reported in various fields such as Li-ion batteries, Al batteries, supercapacitors, fuel cells, photoelectrochemical sensors, field emission electrodes, catalysis, and microwave absorbers.[25,29,38-44] However, despite the enhanced and extended absorption of black TiO_2, most of them do not satisfy the expectation for visible light assisted water splitting.[8,11] This can be attributed to the presence of introduced factors (vide supra), which can also act as negative effects on the photocatalytic activity. For example, oxygen vacancies and/or surface defects are considered one of the important positive factors, act as electron donors to increase donor density and enhance the charge mobility, and help charge separation as a charge trap in black TiO_2.[6,8] However, the high concentration of surface defects and/or oxygen vacancies can also act as recombination centers rather than charge trap, which disturb charge separation and eventually decrease the photocatalytic activity.[8] Recently, Chen et al. published a review article about black TiO_2 materials which describe the synthetic methods and the improved different properties of black TiO_2 materials. It was suggested that ‘‘more efforts are needed from synthesis to property and application in order to finally improve the efficiency of black TiO_2 nanomaterials for practical applications in renewable energy, environment, and others’’.[11] Therefore, finding appropriate synthetic method to prepare a black TiO_2 material with optimized properties for visible light photocatalysis is highly desired. Herein, we report new approach to prepare black TiO_2 nanoparticles for enhanced photocatalytic hydrogen production in the methanol-water system by magnesiothermic reduction in the presence of H_2/Ar for the first time followed by acid treatment to remove Mg species. The magnesiothermic reaction has been used on the industry as a reduction chemical process like reduction of silica to silicon. Titanium chloride ($TiCl_x$) can be reduced metallic titanium in the presence of magnesium at high temperature, and the process is called the Kroll process.[45] Present work is inspired from this process.

II. EXPERIMENTAL DETAILS

2.1 Materials

All of the chemicals are purchased and used without further purification including titanium(IV) dioxide powder (TiO_2, anatase, <25nm, 99.7%, Sigma-Aldrich), Magnesium powder (Mg, SAMCHUN chemical), magnesium hydride (MgH_2, 98%, Alfa Aesar), hydrochloric acid (HCl, 36%, SAMCHUN chemical), and gas mixture of H_2 and Ar (5% H_2 in Ar, AIRTEC Co., Ltd).

2.2 Preparation of Titania Based Photocatalyst

Preparation of H doped titania ($H:TiO_{2-x}$) using Mg and H_2/Ar mixture gas

Commercial anatase white TiO_2 (CT) was mixed with magnesium powder in a molar ratio range between 0.3 and 1.0 by vortex mixer. The well mixed sample was placed in a tube furnace and then heated at 650°C for 5 h under flow of 5% H_2/Ar gas. After heat treatment, the sample was stirred to etch out magnesium species in 2.0 M HCl solution for 24 h. The sample was centrifuged and washed with sufficient water to remove the acid and magnesium species. The washed sample was dried for the characterization in a electric oven at 60°C. The prepared reduced titania samples were denoted as rT-X (where X(=0.3, 0.5, 0.6, 0.75, 1) depends on the molar ratio of TiO_2 and Mg. For comparison study of atmosphere gas effect, different samples are also prepared. The CT was annealed at 650°C under the argon to study the effect of heat and Ar, and the prepared sample was denoted as CT-Ar. The CT was annealed at 650°C under 5% H_2/Ar mixture gas to study the effect of hydrogen, and the sample denoted as CT-H. The CT was annealed in the presence of Mg powder (0.5 mol ratio) at 650°C under Ar to study the effect of Mg in the absence of H_2, and the sample denoted as rT-0.5-Ar.

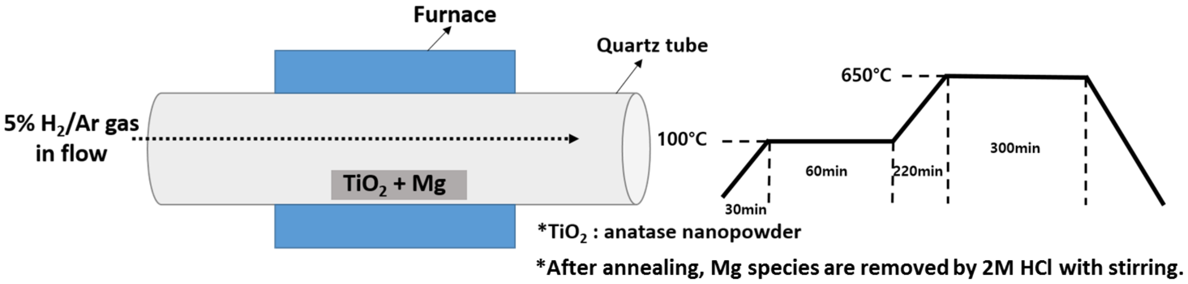

Preparation of H doped titania (H:TiO_{2-x}) using MgH_2

The CT was well-mixed with desired amount of magnesium hydride. The mixed sample was put in a tube furnace and heated at 500°C for 8 h. After annealing, the sample was stirred in a 2.0 M HCl solution for 24 h. The sample was washed with sufficient water and then dried at 60°C. The sample was prepared by using the 0.5 molar ratio of MgH_2, and denoted as rT-MH-0.5

Photo-deposition of Pt nanoparticles

20 mg of TiO_2 catalyst was dispersed in 20% 50 ml of methanol-water solution in a closed Ar gas circulation system. A desired amount of $H_2PtCl_6 \cdot 6H_2O$ was added. The UV light irradiation was obtained from a 450 W Xenon lamp and used for the deposition of Pt under Ar atmosphere. The freshly prepared Pt-deposited catalyst was used as it is for further study.

2.3 Characterization

Characterization techniques

The powder X-ray diffraction (XRD) pattern of the samples was recorded using a Rigaku Smartlab diffractometer with Cu-Kα (0.15406 nm) operated at 40 kV and 30 mA at a scan rate of $4° \cdot min^{-1}$. Raman spectra of the samples were obtained from a Raman spectrometer (NICOLET ALMECA XR, Thermo Scientific) using 532 nm laser beam for excitation. High-resolution transmission electron microscope (HR-TEM) and high-resolution scanning electron microscope (HR-SEM) images were collected using JEOL FE-2010, operated at 300 kV. The ultraviolet-visible-near infrared diffuse reflectance spectra (UV-VIS-NIR DRS) of the samples were recorded by using a UV-VIS-NIR spectrophotometer (CARY 5000, Agilent Technologies). X-ray photoelectron spectroscope (XPS) spectra of the samples were collected using an ESCALAB 250 XPS System with a monochromated Al Kα (150 W) source. The photoluminescence spectra were obtained from a Cary Eclipse Fluorescence Spectrophotometer (Agilent Technologies). The nitrogen adsorption–desorption isotherms of the samples were measured at -196 °C using a Micromeritics ASAP 2460 accelerated surface area and porosity analyzer after the samples were degassed at 150 °C to 20 mTorr for 12 h. The specific surface area was determined based on Brunauer–Emmett–Teller (BET) method from nitrogen adsorption data in the relative pressure range from 0.05 to 0.2.

Band gap calculation

The band gap of the samples was calculated using Tauc plot of $(\alpha h\nu)^2$ vs $h\nu$, where α is the absorption coefficient, h is Plank constant, ν is the wavenumber. The value of $h\nu$ is obtained by converting the wavelength (λ) value. The energy band gap (Eg) is obtained from the intercept of the extrapolated linear part of the curve with the energy axis. The valence band top position was obtained from the VB XPS plot and conduction band bottom was calculated by subtracting the band gap value. The probable band structure was portrayed in potential vs NHE energy diagram.

Photocatalytic H_2 generation

10 mg of photocatalyst loaded with ~1 wt% Pt was added to an aqueous methanol solution (50 ml, 20%) in a closed gas circulation system. The full solar wavelength light irradiation was

obtained from a 400 W Xenon lamp (Newport) embedded with IR filter. Methanol was used as a sacrificial reagent, and the anodic reaction generating O_2 from H_2O did not occur. The amount of H_2 generated was determined by online gas chromatography (Bruker 450 GC) system connected to the reactor. The reaction was carried out at room temperature (25 °C) under Ar atmosphere. For visible light (400 to 780 nm, obtained by using a cutoff filter), 25 mg photocatalyst was used and keeping all other parameters constant. The stability of the catalyst system was studied under the full solar wavelength of light using identical reaction condition as stated above. The solution was stored in the normal ambient condition and irradiated by light for 2 h everyday up to 10 days. Then the solution was again stored for another 20 days and studied again. Before each run, the volume of the solution was made up by adding extra methanol to the solution.

III. RESULTS AND DISCUSSION

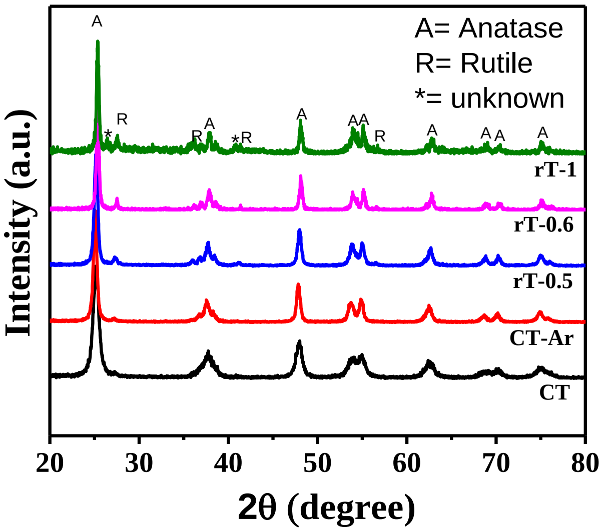

Fig. 1 Powder X-ray diffraction patterns of different samples

The XRD patterns of the various prepared samples confirm mainly anatase phase which is not much changed the crystal phase of the TiO_2 before and after annealing. After annealing, it shows low intensity of extra peaks which mean a little amount of rutile phase. One of main reason of the appearance of rutile phase is heating at 650°C. Not only Mg treated samples but also annealed samples without Mg in argon atmosphere show rutile phase. It means that heat treatment is affect to the formation of the rutile phase. Furthermore, the peak intensities of rutile are increased with the increase of Mg amount, which may indicate that the transformation of anatase to rutile can be facilitated by the presence of Mg at high temperature. No other peak such as related to Mg or MgO is observed except for titania peaks in the XRD pattern, which indicate that Mg species were well-removed after acid-treatment. There is not any peak related to Ti_2O_3 or any other titanium sub-oxide. Although a few unknown peaks are observed in the rT-0.75 and rT-1, all the samples show similar peak pattern. The unknown peaks are not related to MgO, Ti_2O_3 or Mg_2TiO_4.

Scherrer equation	Sample	Dp (nm)
$D_p = \frac{0.94\lambda}{\beta_{1/2}\cos\theta}$ Where Dp = Average Crystallite size, β = Line broadening in radians. θ = Bragg angle λ = X-ray wavelength	CT	10.77
	CT-Ar	16.09
	rT-0.3	16.68
	rT-0.5	15.36
	rT-0.6	21.43
	rT-0.75	25.78
	rT-1	26.36

Table.1 The calculated crystallite size using the Scherrer equation from XRD data

Using Scherrer equation, we calculate the crystallite size of the samples from XRD data. After annealing, the crystallite size of the samples is higher than pristine TiO_2. The crystallite size of the rT-0.3, rT-0.5 and CT-Ar is similar, which may indicate that the increment of crystallite size for rT-0.3 and rT-0.5 is due to heat during annealing. In case of higher amount (mole ratio > 0.5) of Mg treatment, it shows that the crystallite size increases as increasing the amount of Mg. It may indicate that the increment of crystallite size is induced by doping of Mg.

The XRD analysis shows that there is no major structural change during magnesiothermic reduction except the formation of a little rutile phase. Despite of the XRD data, it can be supposed that Mg changes the surface of the TiO_2 particle, which induces color variation from white to light gray to dark black as increasing Mg.

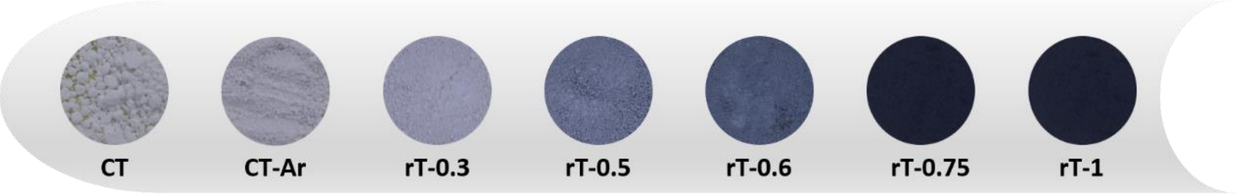

Fig. 2 Images of different samples showing corresponding color.

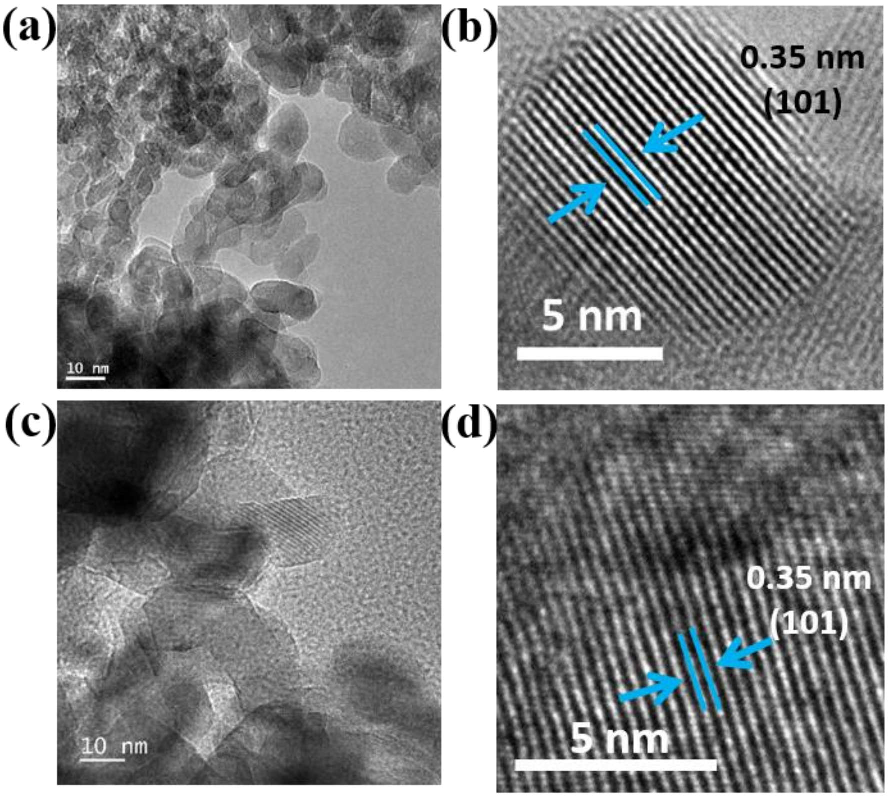

Fig. 3 HR-TEM images of CT (a and b) and BT-0.5 (c and d).

By high-resolution transmittance microscopy (HR-TEM) analysis, the morphology of commercial TiO_2 (CT) and reduced black titania (rT) was studied. According to the images, the particle size of CT and rT-0.5 is about 10-20 nm. It shows around 10-15 nm of particle size for CT, whereas 15-20 nm for rT-0.5. It is well-matched with the calculated value from XRD data. Both CT and rT-0.5 show 0.35 nm of lattice distance, which corresponds to the (101) plane of anatase phase. After magnesiothermic reduction, the lattice fringe distance is maintained and {101} facet is exposed for reduced titania, which indicates that the exposed {101} facet of the pristine anatase TiO_2 remains unchanged. Which facet of TiO_2 is mainly exposed is one of critical factors for its photocatalytic performance. Depends on the facet, photocatalytic activity is affected as the surface atomic configuration and coordination effect the adsorption and reactivity because of difference of surface energy.[49] Because {001} facets have the highest surface energy, {101} facets are thermodynamically more stable than {001} facets in case of anatase TiO_2, which indicates that {001} facets are more reactive than {101} facets. However, after loading of Pt as a co-catalyst, {101} facets show the highest activity for the hydrogen production as a result of water splitting.[46]

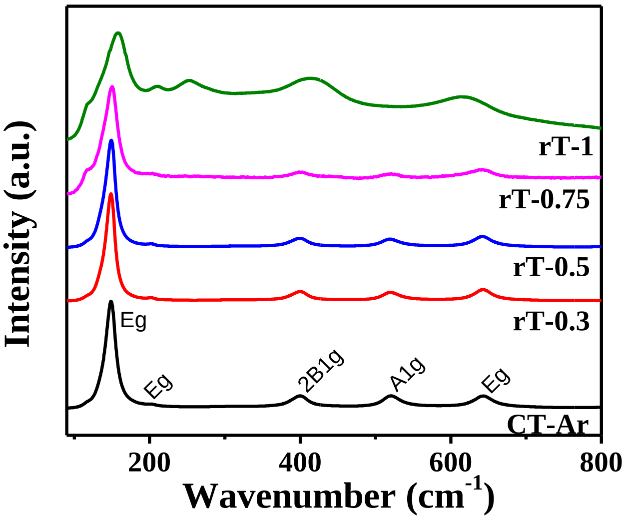

Fig. 4 Raman spectra of the different samples.

By Raman spectroscopy, the surface of reduced black TiO_2 was further investigated. In the Raman spectrum, the annealed CT-Ar shows 6 characteristic Raman bands, which indicates 3Eg + $2B_{1g}$ + A_{1g}. These are typical Raman bands of typical anatase phase and it shows the strongest Eg band around at 148 cm^{-1}. By peak broadening for reduced TiO_2 samples compared with CT-Ar, the band exhibits a blue shift. This phenomenon was reported in the other reports and attributed to non-stoichiometry over the surface of modified titania samples.[5-7,19,33] It is directly correlated to oxygen deficiency at the surface. It can be considered the lattice regularity and the octahedral symmetry of TiO_6 are destroyed on the surface during magnesiothermic reduction. For the rT-1 sample, it shows a distorted spectrum which have extra peaks and different shape compared with other samples. It may be attributed to the over-reduction and phase transition anatase to rutile in the presence of a high amount of Mg.

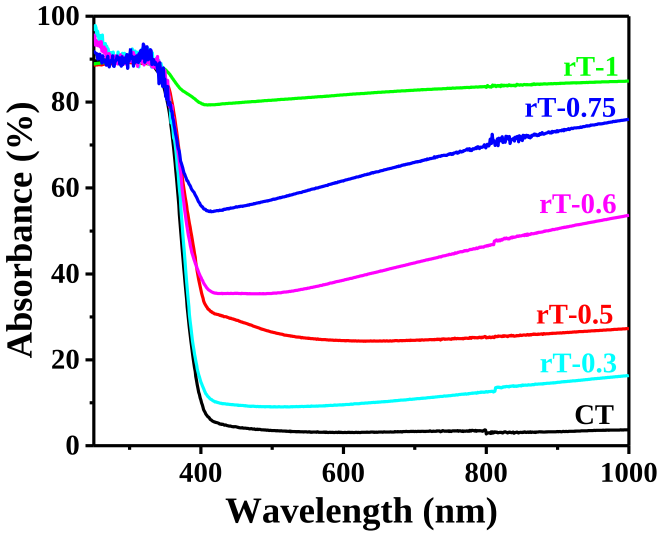

Fig. 5 Absorbance spectra of different samples.

The absorption spectra show the absorption variation of prepared samples as increasing the amount of Mg. The reduced samples exhibit sharp absorption peak shifting to around 420 nm and also display an extended slope. Pristine TiO_2 only absorb ultraviolet (UV) light, whereas Mg treated reduced samples exhibit extended absorption from UV to visible (VIS) and infrared (IR) region. The absorption of light is enhanced as increasing the amount of Mg as observed for the different samples. The extended and enhanced absorption is well correlated to the color change trend of samples from white to gray and black, which indicates that there is surface modification on the TiO_2 particle after magnesiothermic treatment.

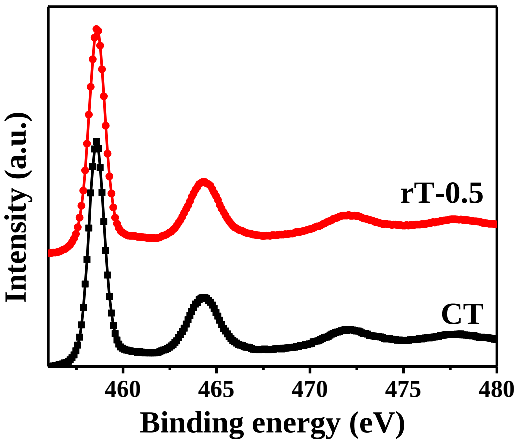

Fig. 6 High-resolution XPS for Ti 2p of CT and BT-0.5 samples.

To further study of reduced TiO_2, X-ray photoelectron spectroscopy (XPS) was used. In the high-resolution XPS spectra, there are two strong peaks at 458.5 and 464.3 eV (Ti $2p_{3/2}$ and $2p_{1/2}$, respectively), which indicate the presence of Ti^{4+} for CT and rT-0.5. The spectra of CT and rT-0.5 is almost similar, which means that these have a similar bonding environment. It makes confirm that there are not any impurities like Mg or carbon after magnesiothermic treatment of pristine TiO_2.[5,33] We cannot find the evidence of the presence of Ti^{3+} for rT-0.5. However, a well-formed tail towards lower binding energy was observed in the Ti 2p XPS spectrum of rT-1, which indicates the evidence of Ti^{3+}. Extrapolating from this result, Ti^{3+} may be also presence in rT-0.5 in a lower amount.

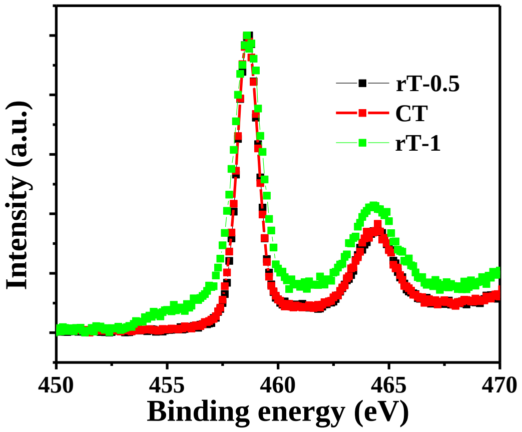

Fig. 7 Ti 2P XPS spectrum of different TiO_2 samples

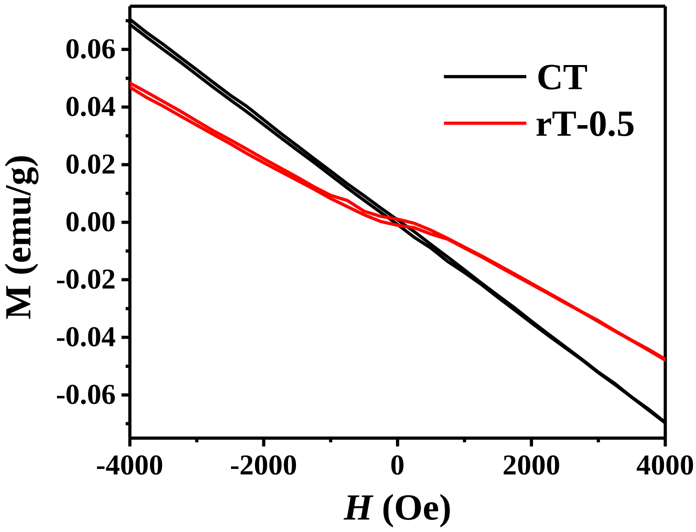

Fig. 8 Magnetic field dependence of magnetization plots of different samples.

To further confirm the presence of Ti^{3+} in rT-0.5, magnetic field dependence of magnetization was investigated. In the electronic configuration, Ti^{3+} is paramagnetic, which indicates that the presence of Ti^{3+} can introduces ferromagnetism, and it is measured by the plot of magnetic field dependence of magnetization.[33] The pristine TiO_2 (CT) show no hysteresis, whereas a clear hysteresis was observed for the rT-0.5 and rT-1, which prove the introduction of the ferromagnetic properties caused by the formation of Ti^{3+} in prepared samples during reduction. By the presence of ferromagnetism and the tailed XPS spectrum, we can confirm the presence of Ti^{3+} in synthesized black TiO_2 indirectly.

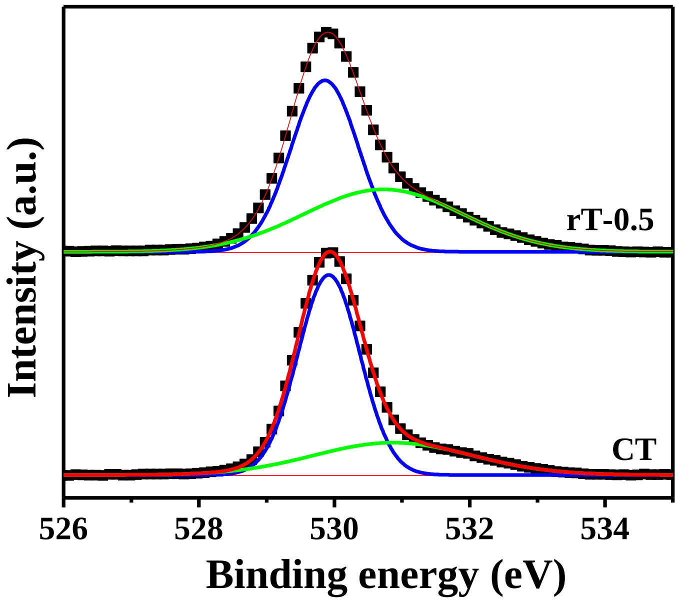

Fig. 9 High-resolution XPS for O 1s of CT and BT-0.5 samples.

The HR-XPS spectra of O 1s are well deconvoluted to two peaks, which indicate a quite sharp peak at 529.8 eV, and a quite broad peak at higher binding energy of 531 eV. The lattice oxygen of TiO_2 attribute to the peak at 529.8 eV, whereas the peak at higher binding energy, 531 eV, is result in the presence of Ti-OH groups at the surface. The broad peak can be correlated with the oxygen vacancy or surface defects caused by reduction. Compared with pristine TiO_2, the area of the peak at higher binding energy is larger for rT-0.5. As increasing the amount of Mg, the peak intensity also increases. This can be understood as more oxygen vacancies or surface defects formed during the magnesiothermic reduction of TiO_2.

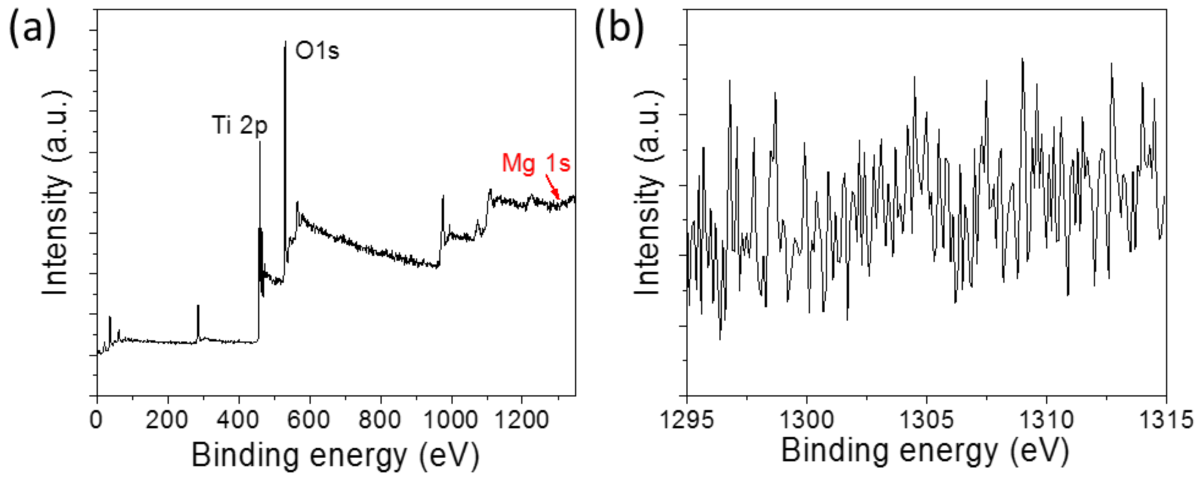

Fig. 10 Full XPS survey (a) and Mg 1s scan (b) of sample BT-0.5

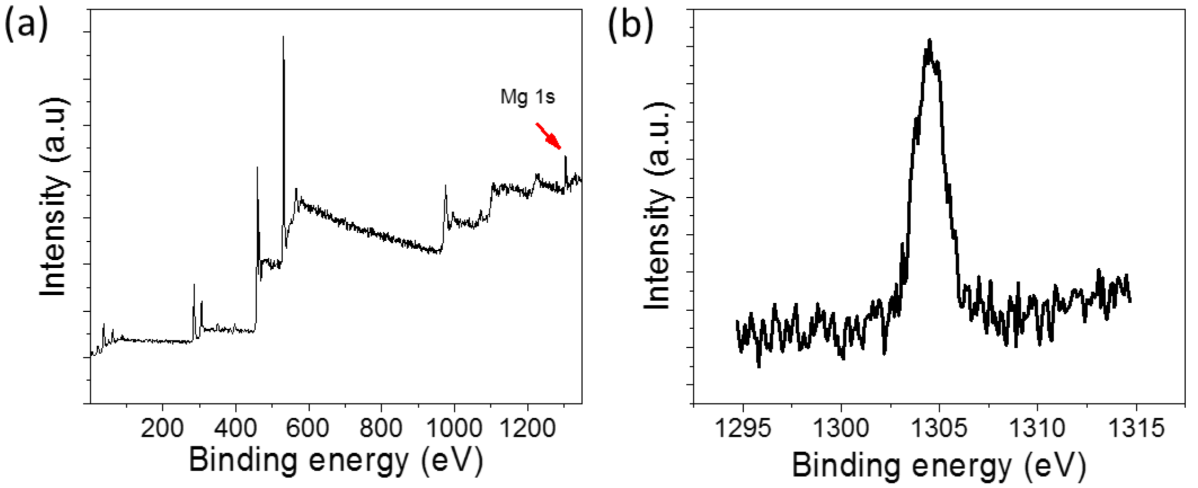

Fig. 11 Full XPS survey (a) and Mg 1s scan (b) for sample BT-1

The full XPS survey has to be announced to know whether the Mg species were removed or not. The full XPS spectrum of rT-0.5 does not show any peaks related to Mg, which confirm that Mg is fully removed during etching process, whereas the presence of Mg is observed in case of rT-1. For rT-1, the XPS profile of Mg 1s exhibits a peak at 1304.5 eV which corresponds to Mg ion related to oxygen. There is no peak which corresponds to MgO in the XRD. It means there is possibility of doping of Mg^{2+} ion to titanium oxide. Mg^{2+} ion may dope to the lattice or surface of titanium oxide, which also consistent with the increment of crystallite size of rT-1 as the greater ionic radius of Mg^{2+} than Ti^{4+}.

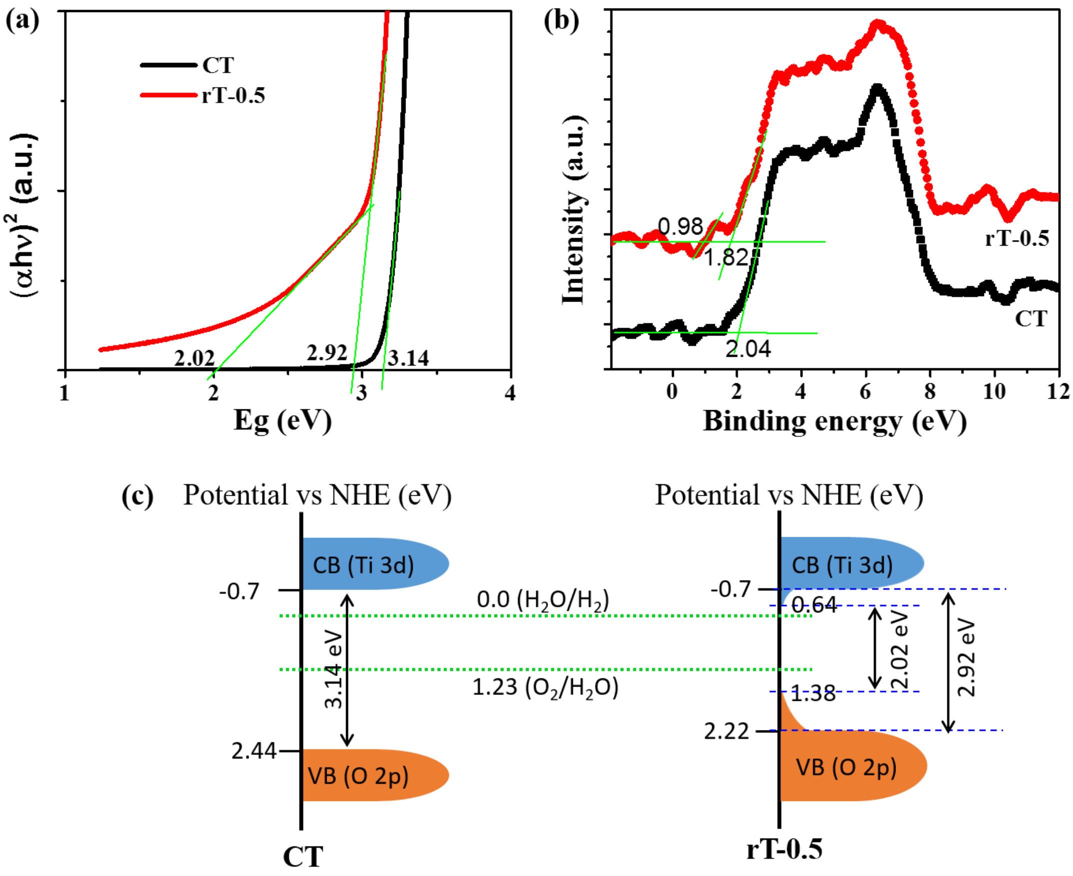

Fig. 12 (a) Tauc plot for band gap determination, (b) VB XPS of the samples, and (c) band energy diagram

The band gap of CT and rT-0.5 was calculated from Tauc plot obtained from absorption spectrum by DRS method. The calculated band gap is 3.14 eV for CT, whereas two band gap values are observed for rT-0.5, which corresponds to two slope in the absorption spectrum. The obtained values are 2.92 and 2.02 eV in the Tauc plot for rT-0.5. The lower band gap value for rT-0.5 indicates the presence of a tail of the valence band (VB) top, which means introduction of a new density of states (DOS).[19] By VB XPS spectra of samples, the VB position was also further studied. The VB top position for CT is observed at 2.04 eV, whereas the VB XPS of rT-0.5 shows the position of VB top at 1.82 eV and 0.98 eV. It indicates that the VB for rT-0.5 shifts 0.22 eV and forms a tail state up to 1.06 eV upward. Compare with CT, rT-0.5 shows two different band gap, and the maximum band gap difference of CT and rT-0.5 is 1.02 eV, which indicates the presence of another tail state to the downward from the conduction band (CB) for rT-0.5. A schematic band position for CT and rT-0.5 can be portrayed in the potential vs. NHE energy diagram by combining the above results. The newly introduced tail states which are upward shifted VB top and downward shifted CB bottom are due to the modified surface defects or oxygen vacancies and the presence of Ti^{3+}, respectively, inducing to reduce band gap and showing enhanced and extended light absorption and improved photocatalytic activity.

Pt nanoparticle was deposited on the surface of titanium oxide particle as a co-catalyst. The deposited Pt was confirmed by XPS and HR-TEM analysis of the Pt loaded rT-0.5 sample.

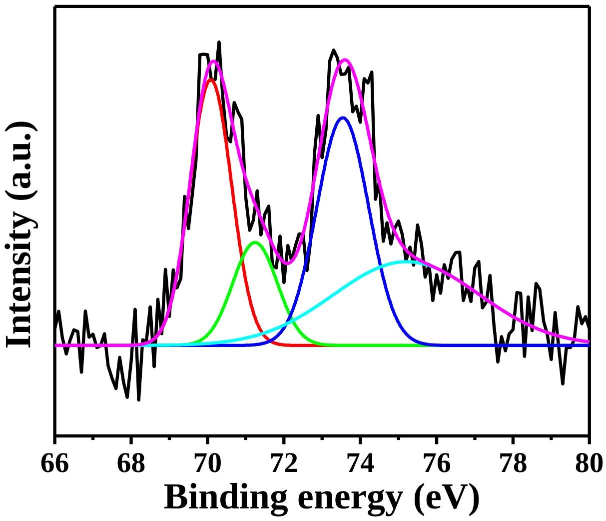

Fig. 13 XPS spectrum of Pt 4f for rT-0.5 sample after Pt deposition under UV light.

There are three different types of Pt species and the presence of them is confirmed by Pt 4f XPS spectrum. The highest intensity components have spin-orbit split binding energies at 70.1 and 73.6 eV, which confirm that metallic Pt (0) states present predominantly. The other two peaks which are green and sky-blue line in the Fig. 13 are correlated to the presence of Pt(II)O and Pt(IV)O_2 species in the samples. The number ratio of loaded Pt to TiO_2 is 0.9%.

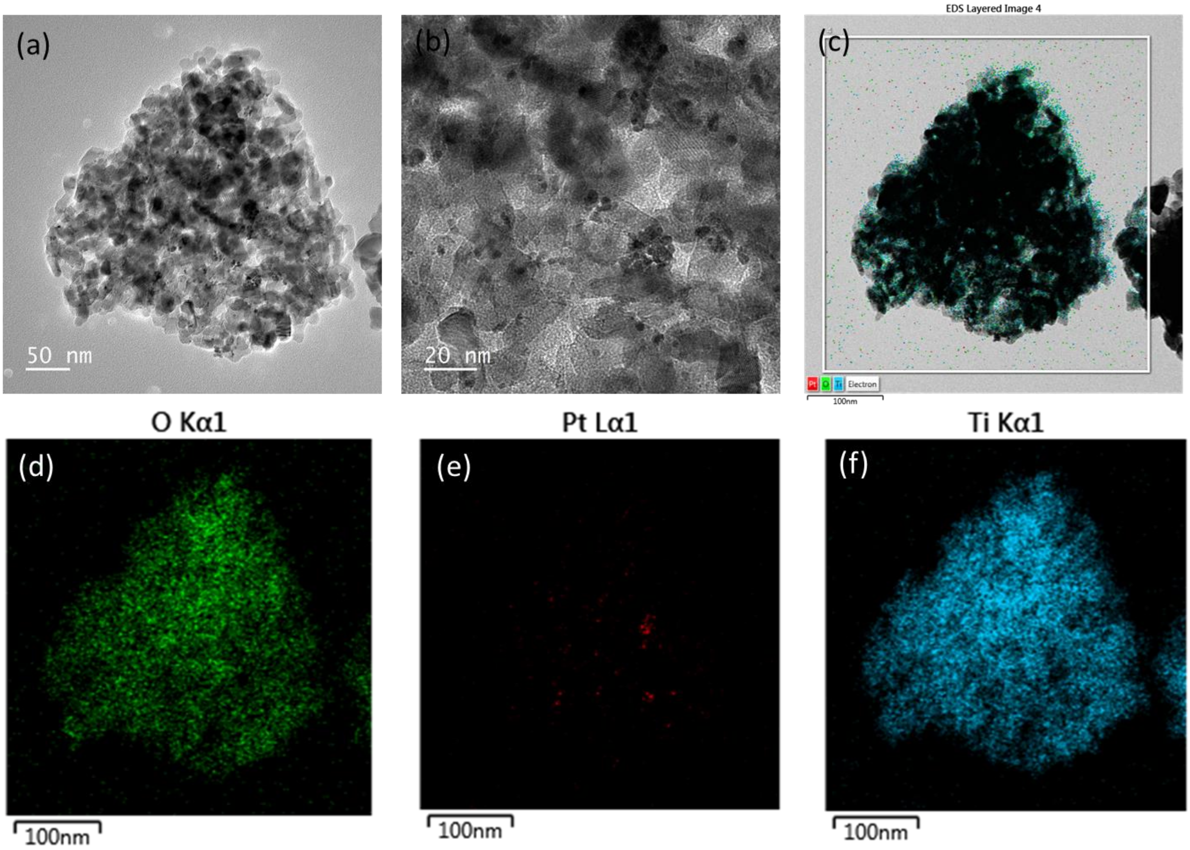

Fig. 14 HR-TEM images (a and b) and EDS elemental mappings (c-f) of Pt-deposited rT-0.5. The (c) shows the EDS layered image containing image mappings for all elements.

In the HR-TEM images, well-dispersed small nanoparticles (~nm) are observed on the rT-0.5, which indicates that Pt nanoparticles are homogeneously deposited. Elemental mapping further confirm the homogeneous distribution of Pt nanoparticles.

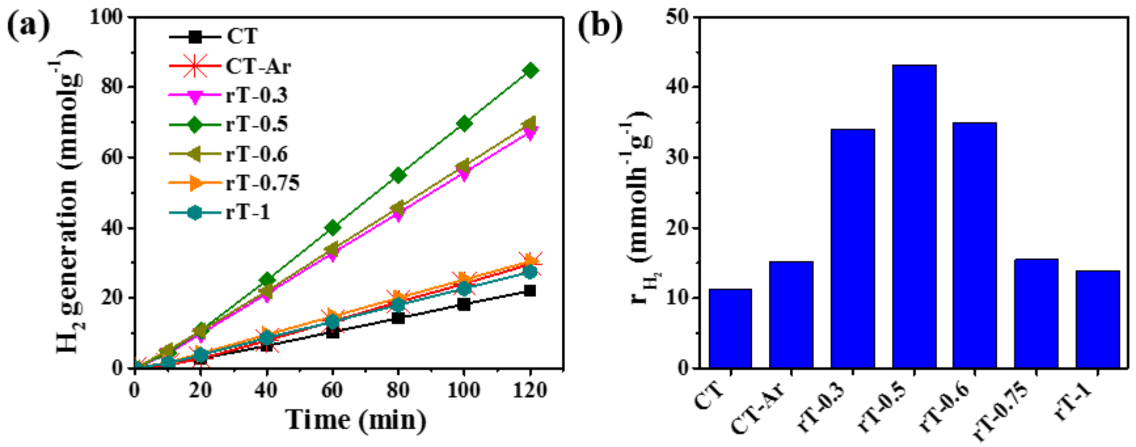

Fig. 15 H_2 generation profile (a) and rate (r_{H2}) of hydrogen generation (b) for different samples under the full solar wavelength range of light

The hydrogen production is measured by gas chromatography (GC). The continuous hydrogen production profile and the rate of H_2 production for different samples under the full solar wavelength range of light are shown. The rate of hydrogen production is increased for all the prepared annealed samples and, especially, Mg treated samples show significant increment. A maximum 43.2 mmol·h^{-1}·g^{-1} of H_2 production rate is observed for rT-0.5 sample. This value is really notable and is 3 to 20 times higher than the rates of similar reported black TiO_2 samples. Table 2 is the list of reported results.

Black TiO_2 photocatalyst	Reactant solution	Co-catalyst	Light source	Rate of hydrogen generation	
				Full solar wavelength of light ($mmolh^{-1}g^{-1}$)	Visible light ($\mu molh^{-1}g^{-1}$)
Hydrogenated Black TiO2[5]	50 % CH_3OH	0.6 % Pt	AM-1.5 solar stimulator	10	100
Hydrogenated titanate nanotube[7]	20 % CH_3OH	1 % Pt	Xe arc lamp, 300 W	2.15	120
Al-reduced black TiO_2[32]	25 % CH_3OH	0.5 % Pt	Hg lamp, 300W	6.4	140
Nonmetal doping Al-reduced black TiO_2[30]	20 % CH_3OH	0.5 % Pt	Xe lamp, 300 W		
TiO2-H				7.4	123
TiO2-N				15	200
TiO2-S				12.1	135
TiO2-I				10.3	160
Al-reduced black S doped rutile TiO_2[34]	50 % CH_3OH	0.5 % Pt	AM 1.5 simulated solar power system	---	258
Ordered mesoporous hydrogenated black TiO_2[9]	20 % CH_3OH	1 % Pt	AM 1.5 solar power system	---	13.6
Current work	20 % CH_3OH	1 % Pt	Xe lamp, 400 W	43.2	440

Table. 2 Rate of hydrogen generation obtained by using different black TiO_2 materials

For the Mg treated samples, the rate increases up to rT-0.5, it starts to decrease for much higher Mg treated samples. Although rT-0.75 and rT-1 show much enhanced light absorption, greater presence of Ti^{3+} and oxygen vacancies, the rate of hydrogen production is less than rT-0.5. It looks unreasonable, but one possibility can be affordable to explain for the odd results, which is the generation of new recombination sites due to over-reduction and Mg^{2+} doping.[30,47] As a result of increased electron-hole recombination, the hydrogen production decreases despite of the high light absorption.

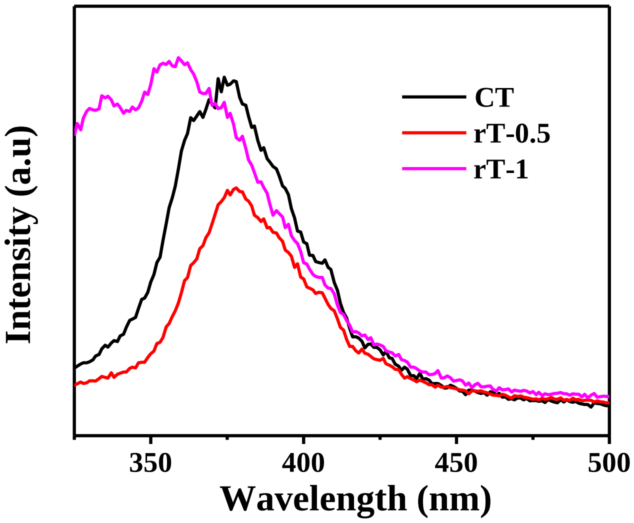

Fig. 16 Photoluminescence (PL) spectra of different samples.

The photoluminescence spectra of different samples show the emission of light which indicates the recombination of electron and hole. The intensity directly is correlated to the degree of recombination and it support the explanation of introduction of new recombination center for rT-0.75 and rT-1. The PL spectra show decreased recombination for rT-0.5, whereas the spectrum for rT-1 show the increased recombination in the broaden range than CT, which is well-matched with the result of H_2 production rate.

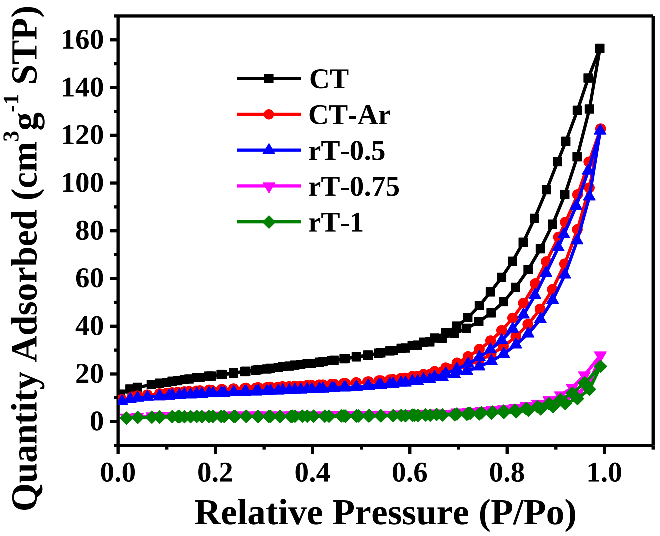

Fig. 17 N_2 adsorption/desorption isotherms for different samples.

Specific surface areas were measured by N_2 adsorption/desorption analysis. In general, it shows that surface area has a tendency to decrease with Mg treatment. After the ratio of 0.5, the isotherms dramatically change with sharp drop of surface area. The obtained surface areas are 69, 40, 36, 12, and 9 m^2g^{-1} for CT, CT-Ar, rT-0.5, rT-0.75, and rT-1, respectively. The surface area of CT is highest and that of CT-Ar and rT-0.5 are similar, which indicates that this decrement is coming from heat treatment. for the sample rT-0.75 and rT-1, the surface area is drastic drop than the other samples. It is can be attributed to the increase in crystallite size as observed in XRD and HR-TEM and may cause the decrease in the rate of hydrogen production. To check the correlation between surface area and the hydrogen production rate, we calculate the rate of hydrogen production normalized with the surface area of the sample. The rate of hydrogen production normalized with surface area are 1.2, 1.3, and 1.5 $mmolh^{-1}m^{-2}$ for rT-0.5, rT-0.75, and rT-1, respectively.

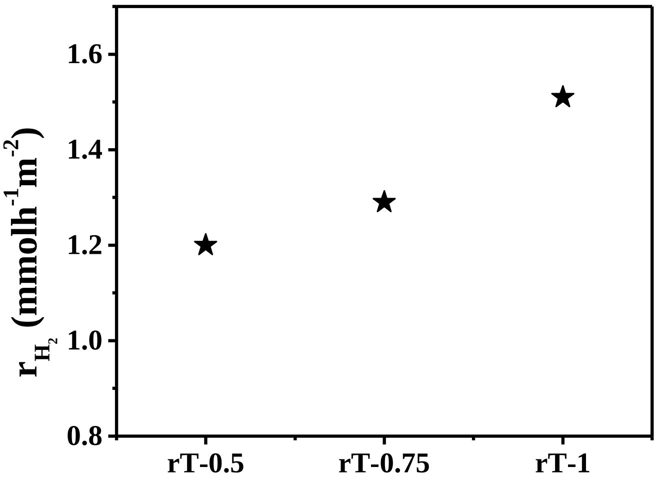

Fig. 18 Rate of surface area-normalized hydrogen generation (r_{H_2}) for different samples.

To calculate the rate of surface area-normalized hydrogen production (mmolh^{-1}m^{-2}), the rate of mass-normalized hydrogen production (mmolh^{-1}g^{-1}) is divided by the specific surface area (m^{2}g^{-1}) of the corresponding sample. The obtained results are as follow.

Sample	Rate of hydrogen production (mmolh^{-1}g^{-1})	Surface area (m^{2}g^{-1})	Rate of hydrogen production (mmolh^{-1}m^{-2})
rT-0.5	43.2	36	1.2
rT-0.75	15.4	12	1.3
rT-1	13.9	9	1.5

The surface area-normalized rate is increased as increasing Mg amount. The tendency of hydrogen production rate is different with non-normalized result. There are several factors control the photocatalytic water splitting, but this results indicates that the decreased surface area is one of main reason for the decrease in the hydrogen production rate for the high amount of Mg treated samples like rT-0.75 or rT-1. The high surface area material has more active sites and Pt nanoparticles can well-distribute on the materials, which induces the overall catalytic activity. Because of decreased surface area, Pt particle size is relatively increased to the material, which may induce the decrease in the efficiency of Pt particles.[48]

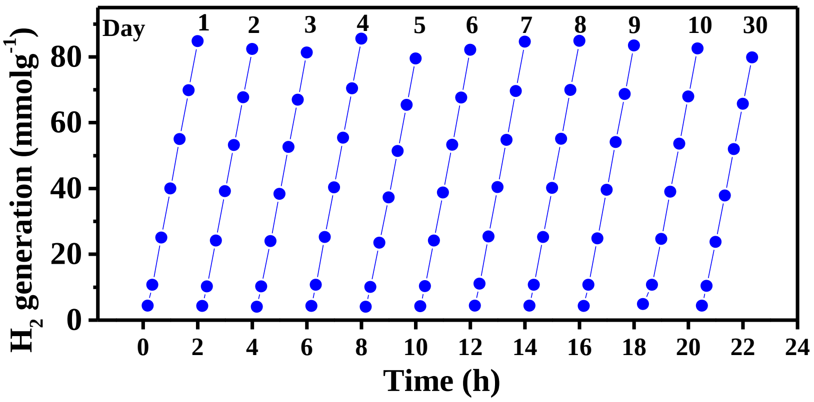

Fig. 19 The stability study of the sample rT-0.5 under the full solar wavelength range of light.

Because the sample rT-0.5 showed remarkable photocatalytic activity, the stability in the light was further studied for hydrogen production under full solar light. There is only negligible change in the photocatalytic hydrogen production in up to 10 cycles, which means that it is remarkably stable. The consistent results were collected from the same solution for successive days. After storing the solution for 1 month, it still shows similar photocatalytic activity. The sample was stored without any capping and no color change was observed for all the prepared samples after three months. In the simultaneous used Mg and H_2 method, both Mg and H_2 act important roles to generate a very active and stable reduced black titania based photocatalyst.

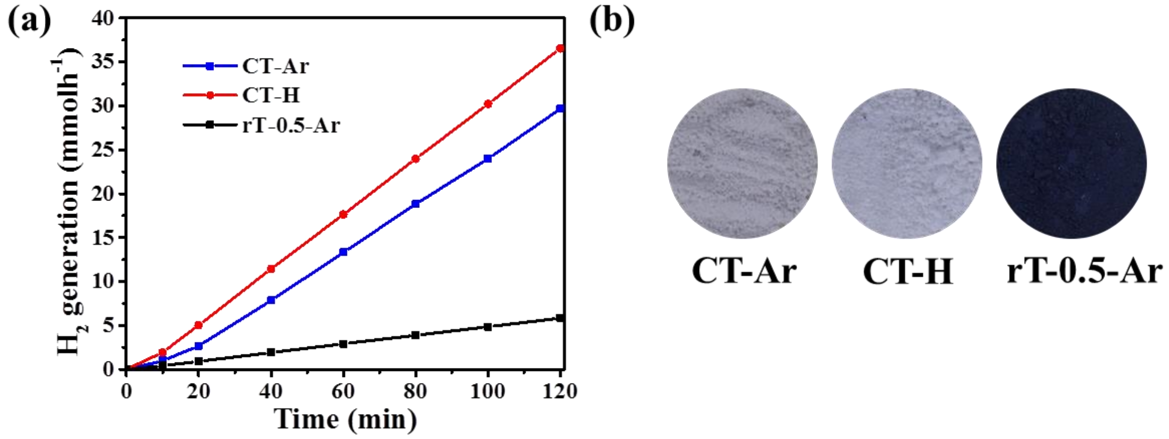

Fig. 20 (a) Hydrogen production profiles and for the samples, CT-Ar, CT-H, and rT-0.5-Ar and (b) color of the corresponding samples.

To investigate the effect of Mg and H_2 during the synthetic procedure on the activity of the modified catalyst, different samples were prepared as shown in Fig. 20 (refer to experimental section). The rates of hydrogen production are 15.2, 18.5, and 3 mmol h^{-1} g^{-1} for the samples of CT-Ar, CT-H, and rT-0.5-Ar, respectively. The activity of CT-H slight increase compared to CT-Ar, and it is hydrogenation of nano TiO_2 materials. The hydrogenation is very light and the effect also less, and the color of sample also still almost white like CT. This indicates the remarkable photocatalytic activity of rT-0.5 is not coming from the mild hydrogenation by lower concentration of hydrogen (5% H_2/Ar gas). On the other hand, the rT-0.5-Ar shows poor photocatalytic activity, and it is less than CT-Ar, even though the color is dark black. This result can be correlated to the activity of rT-1. Therefore, it can be considered the synergy effect of Mg and hydrogen is essential to be the most active photocatalyst.

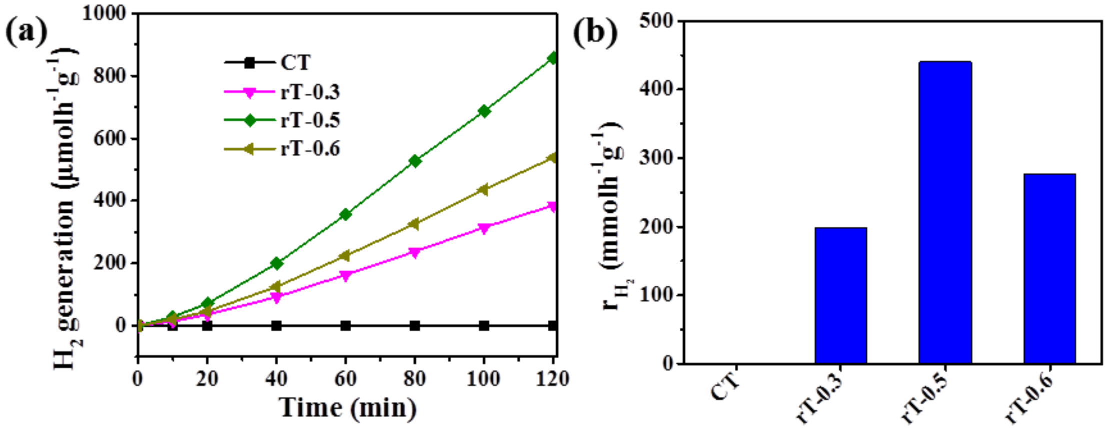

Fig. 21 H_2 generation profile (a) and rate (r_{H2}) of hydrogen generation (b) for different samples under visible light.

The photocatalytic hydrogen production of the prepared samples was studied in the visible light irradiation also. The performance was decreased compare with the case of full solar wavelength range of light irradiation. However, rT-0.5 is still the best sample which shows superior activity of 440 µmol h^{-1} g^{-1} compared with other prepared samples. The pristine CT reveals no activity under visible light. Even though rT-1 sample shows maximum absorbance in visible light, the activity is poor. It may be attributed to the low surface area and the presence of a number of recombination centers due to over-reduction or doping of Mg^{2+} as mentioned above. Furthermore, the photocatalytic activity of prepared reduced TiO_2 sample (rT-0.5) under the irradiation of visible light is also superior to those of previously reported reduced black TiO_2 samples. The reported best rate of hydrogen production was 258 µmol h^{-1} g^{-1} and it was achieved by Al-reduced black S-doped rutile TiO_2.[34] The results indicate that sample rT-0.5 surpass the other reported samples, demonstrating enormously high photocatalytic hydrogen production activity under both full solar wavelength and visible light.

The outstanding activity can be explained with the extended absorption in visible and IR light, optimal band position, the presence of an appropriate amount of Ti^{3+} caused by hydrogen doping and the generation of oxygen vacancies, and slow charge recombination. Even though there is a long discussion on the role of Ti^{3+} in the reduced TiO_2 for photocatalytic reaction, a clear evidence of the presence of Ti^{3+} is observed in prepared active sample. It can be acceptable to understand the presence of Ti^{3+} in the material can help to reduce the recombination of electron and hole pairs. Due to the presence of Ti^{3+}, the slower charge recombination in rT-0.5 is observed in the PL measurement, which may result in remarkable photocatalytic activity. The disordered surface which caused by oxygen vacancy and hydrogen doping is another important factor, which seems to induce enhancement and extension of the light absorption at higher wavelengths and increase the photolysis activity for hydrogen production. The exposed {101} facets, which are most active facets for hydrogen production in the case of Pt loaded, of rT-0.5 can be favorable to the photocatalytic activity. On the basis of these results, it can be considered the controllable magnesiothermic reduction with hydrogen is one of the best ways to prepare highly active and stable TiO_2 based photocatalyst for various applications although it was just tested for hydrogen generation in here. Regardless of the presence of methanol, there is no hydrogen production without Pt co catalyst. This is perhaps because it is difficult to separate charge sufficiently without Pt, and it is easy to recombine electrons and holes. However, in the case of Pt loaded black TiO_2, the presence of methanol is important. Without methanol, there is almost no hydrogen production. In the absence of the hole scavenger, holes are remained and collected on the surface, which cause easy recombination with electron. The sacrificial reagent scavenges the holes, and disturbs the recombination of electrons and holes. To commercialize and utilize in the real life, it is required more attention to optimize the system for the much improved photocatalytic activity and to know the origin of the enhanced photocatalytic activity.

Knowing how to modify the samples and react the reagents is important to understand the results such as activity and any other variations, to improve the properties and to apply to other materials. There is a lot of report that explains the mechanism of metal catalysts such as Pd and Raney Ni as a hydrogenation catalyst. Briefly, the metal catalysts adsorb hydrogen molecules first, and then change the adsorbate to active state. The resulting active hydrogen can easily react with target to be doped with hydrogen. It is expected that Mg act not only reducing agent but also hydrogenation catalyst as like Pd and Ranny Ni.[50] At 650°C, Mg is started to melt and changed to more active state which can reduce the TiO_2 actively inducing oxygen vacancies and surface defects. Hydrogen molecules can adsorb to the active metal, and can be active state to help hydrogen dope to the TiO_2 by Mg and heat. To check the assumption that the active hydrogen is main element during the reducing process, additional experiment was achieved to prepare reduced TiO_2 by MgH_2. The result was impressive and it showed highly enhanced photocatalytic activity for hydrogen production. It is considered that the active hydrogen which is formed during the melting and decomposition of Mg H_2, well worked as a defects inducer and the TiO_2 was well hydrogenated. This result indirectly supports the assumption that the active hydrogen is highly important to induce optimal reduced black TiO_2 during synthesis.

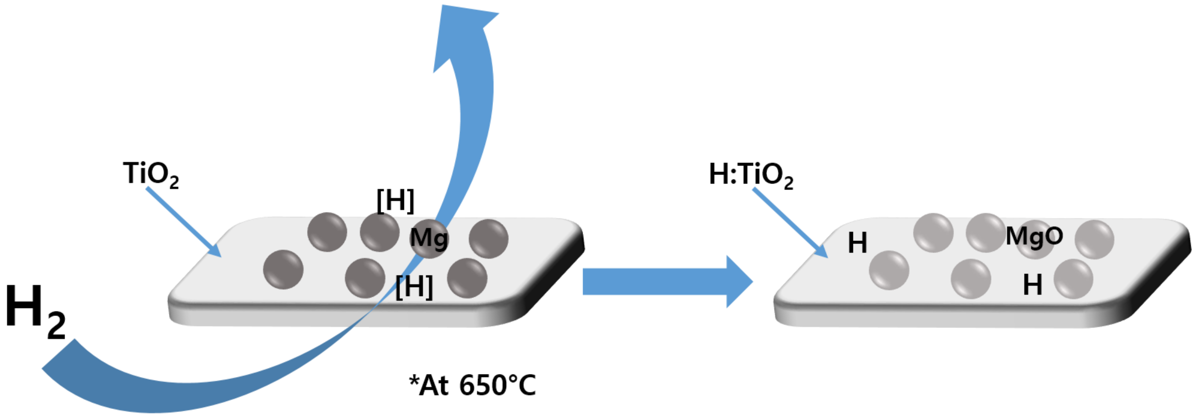

IV. CONCLUSION

The novel approach to prepare a highly active reduced black TiO_2 photocatalyst is dealt in here. The developed synthesis process is the first time to synthesize reduced black TiO_2, which achieved by magnesiothermic reduction in the presence of hydrogen followed by etching process by acid. The prepared TiO_2 catalyst has lower band gap, optimal band position, and slower charge recombination, and shows outstanding photocatalytic hydrogen production performance from methanol-water solution in presence of ~1% Pt as a co catalyst. The maximum rates of hydrogen production are 43 mmol h^{-1} g^{-1} and 440 μmol h^{-1} g^{-1} under full solar wavelength of light and visible light, respectively, and these values are surpassed those of previously reported black TiO_2 materials. The catalyst also shows superb stability up to 30 days, and there is no significant decrement in the activity. We can conclude that the remarkable activity and stability of the black TiO_2 prepared by new developed method are the results of balance of the generated Ti^{3+}, oxygen vacancy, surface defects, and recombination center, which induces optimal band gap and position, during magnesiothermic reduction in the presence of hydrogen. We also suggest the core of induced optimal defects during preparation of reduced black TiO_2 is the activation of hydrogen.

References

1. J. Schneider, M. Matsuoka, M. Takeuchi, J. Zhang, Y. Horiuchi, M. Anpo and D. W. Bahnemann. “Understanding TiO_2 Photocatalysis: Mechanisms and Materials” Chem. Rev., 2014, 114, 9919–9986.
2. M. Ni, M. K. H. Leung, D. Y. C. Leung and K. Sumathy. “A review and recent developments in photocatalytic water-splitting using TiO_2 for hydrogen production” Renewable Sustainable Energy Rev., 2007, 11, 401–425.
3. Y. Qu and X. Duan. “Progress, challenge and perspective of heterogeneous photocatalysts” Chem. Soc. Rev., 2013, 42, 2568–2580.
4. A. Dhakshinamoorthy, S. Navalon, A. Corma and H. Garcia. “Photocatalytic CO_2 reduction by TiO_2 and related titanium containing solids” Energy Environ. Sci., 2012, 5, 9217–9233.
5. X. Chen, L. Liu, P. Y. Yu and S. S. Mao. “Increasing solar absorption for photocatalysis with black hydrogenated titanium dioxide nanocrystals” Science, 2011, 331, 746–750.
6. G. Wang, H.Wang, Y. Ling, Y. Tang, X. Yang, R. C. Fitzmorris, C.Wang, J. Z. Zhang and Y. Li. “Hydrogen-treated TiO_2 nanowire arrays for photoelectrochemical water splitting” Nano Lett., 2011, 11, 3026–3033.
7. Z. Zheng, B. Huang, J. Lu, Z. Wang, X. Qin, X. Zhang, Y. Dai and M.-H. Whangbo. “Hydrogenated titania: synergy of surface modification and morphology improvement for enhanced photocatalytic activity” Chem. Commun., 2012, 48, 5733–5735.
8. Y. H. Hu. “A Highly Efficient Photocatalyst—Hydrogenated Black TiO_2 for the Photocatalytic Splitting of Water” Angew. Chem., Int. Ed., 2012, 51, 12410–12412.
9. W. Zhou, W. Li, J.-Q. Wang, Y. Qu, Y. Yang, Y. Xie, K. Zhang, L. Wang, H. Fu and D. Zhao. “Ordered mesoporous black TiO_2 as highly efficient hydrogen evolution

photocatalyst" J. Am. Chem. Soc., 2014, 136, 9280–9283.

10. S. Hoang, S. P. Berglund, N. T. Hahn, A. J. Bard and C. B. Mullins. "Enhancing visible light photo-oxidation of water with TiO_2 nanowire arrays via co treatment with H_2 and NH_3: synergistic effects between Ti^{3+} and N" J. Am. Chem. Soc., 2012, 134, 3659–3662.
11. X. Chen, L. Liu and F. Huang. "Black titanium dioxide (TiO_2) nanomaterials" Chem. Soc. Rev., 2015, 44, 1861–1885.
12. H. Lu, B. Zhao, R. Pan, J. Yao, J. Qiu, L. Luo and Y. Liu. "Safe and facile hydrogenation of commercial Degussa P25 at room temperature with enhanced photocatalytic activity" RSC Adv., 2014, 4, 1128–1132.
13. N. Liu, C. Schneider, D. Freitag, M. Hartmann, U. Venkatesan, J. Mu¨ller, E. Spiecker and P. Schmuki. "Black TiO_2 nanotubes: cocatalyst-free open-circuit hydrogen generation" Nano Lett., 2014, 14, 3309–3313.
14. C. Sun, Y. Jia, X.-H. Yang, H.-G. Yang, X. Yao, G. Q. Lu, A. Selloni and S. C. Smith. "Hydrogen incorporation and storage in well-defined nanocrystals of anatase titanium dioxide" J. Phys. Chem. C, 2011, 115, 25590–25594.
15. X. Yu, B. Kim and Y. K. Kim. "Highly enhanced photoactivity of anatase TiO_2 nanocrystals by controlled hydrogenation-induced surface defects" ACS Catal., 2013, 3, 2479–2486.
16. Y. Zhu, D. Liu and M. Meng. "H_2 spillover enhanced hydrogenation capability of TiO_2 used for photocatalytic splitting of water: a traditional phenomenon for new applications" Chem. Commun., 2014, 50, 6049–6051.
17. J. Qiu, S. Li, E. Gray, H. Liu, Q.-F. Gu, C. Sun, C. Lai, H. Zhao and S. Zhang. "Hydrogenation synthesis of blue TiO_2 for high-performance lithium-ion batteries" J. Phys. Chem. C, 2014, 118, 8824–8830.

18. G. Li, Z. Zhang, H. Peng and K. Chen. “Mesoporous hydrogenated TiO_2 microspheres for high rate capability lithium ion batteries” RSC Adv., 2013, 3, 11507–11510.
19. A. Naldoni, M. Allieta, S. Santangelo, M. Marelli, F. Fabbri, S. Cappelli, C. L. Bianchi, R. Psaro and V. Dal Santo. “Effect of nature and location of defects on bandgap narrowing in black TiO_2 nanoparticles” J. Am. Chem. Soc., 2012, 134, 7600–7603.
20. Z. Liang, G. Zheng, W. Li, Z. W. Seh, H. Yao, K. Yan, D. Kong and Y. Cui. “Sulfur cathodes with hydrogen reduced titanium dioxide inverse opal structure” ACS Nano, 2014, 8, 5249–5256.
21. Z. Wei-Dong, W. Cheng-Wei, C. Jian-Biao, L. Dong-Sheng, Z. Feng and Z. Hao-Li. “Enhanced field emission from hydrogenated TiO_2 nanotube arrays” Nanotechnology, 2012, 23, 455204.
22. J.-Y. Shin, J. H. Joo, D. Samuelis and J. Maier. “Oxygen-deficient $TiO_{2-\delta}$ nanoparticles via hydrogen reduction for high rate capability lithium batteries” Chem. Mater., 2012, 24, 543–551.
23. A. Danon, K. Bhattacharyya, B. K. Vijayan, J. Lu, D. J. Sauter, K. A. Gray, P. C. Stair and E. Weitz. “Effect of reactor materials on the properties of titanium oxide nanotubes” ACS Catal., 2012, 2, 45–49.
24. H. He, K. Yang, N. Wang, F. Luo and H. Chen. “Hydrogenated TiO_2 film for enhancing photovoltaic properties of solar cells and self-sensitized effect” J. Appl. Phys., 2013, 114, 213505.
25. S.-T. Myung, M. Kikuchi, C. S. Yoon, H. Yashiro, S.-J. Kim, Y.-K. Sun and B. Scrosati. “Black anatase titania enabling ultra-high cycling rates for rechargeable lithium batteries” Energy Environ. Sci., 2013, 6, 2609–2614.
26. X. Chen, L. Liu, Z. Liu, M. A. Marcus, W.-C. Wang, N. A. Oyler, M. E. Grass, B. Mao, P.-A. Glans, P. Y. Yu, J. Guo and S. S. Mao. “Properties of disorder-engineered black

titanium dioxide nanoparticles through hydrogenation" Sci. Rep., 2013, 3, 1510.

27. I. S. Cho, M. Logar, C. H. Lee, L. Cai, F. B. Prinz and X. Zheng. "Rapid and controllable flame reduction of TiO_2 nanowires for enhanced solar water-splitting" Nano Lett., 2013, 14, 24–31.

28. J. Dong, J. Han, Y. Liu, A. Nakajima, S. Matsushita, S. Wei and W. Gao. "Defective black TiO_2 synthesized via anodization for visible-light photocatalysis" ACS Appl. Mater. Interfaces, 2014, 6, 1385–1388.

29. Y. J. He, J. F. Peng, W. Chu, Y. Z. Li and D. G. Tong. "Black mesoporous anatase TiO_2 nanoleaves: a high capacity and high rate anode for aqueous Al-ion batteries" J. Mater. Chem. A, 2014, 2, 1721–1731.

30. T. Lin, C. Yang, Z. Wang, H. Yin, X. Lu, F. Huang, J. Lin, X. Xie and M. Jiang. "Effective nonmetal incorporation in black titania with enhanced solar energy utilization" Energy Environ. Sci., 2014, 7, 967–972.

31. T. Nakajima, T. Nakamura, K. Shinoda and T. Tsuchiya. "Rapid formation of black titania photoanodes: pulsed laser-induced oxygen release and enhanced solar water splitting efficiency" J. Mater. Chem. A, 2014, 2, 6762–6771.

32. Z. Wang, C. Yang, T. Lin, H. Yin, P. Chen, D. Wan, F. Xu, F. Huang, J. Lin, X. Xie and M. Jiang. "H-Doped Black Titania with Very High Solar Absorption and Excellent Photocatalysis Enhanced by Localized Surface Plasmon Resonance" Adv. Funct. Mater., 2013, 23, 5444–5450.

33. Z. Wang, C. Yang, T. Lin, H. Yin, P. Chen, D. Wan, F. Xu, F. Huang, J. Lin, X. Xie and M. Jiang. "Visible-light photocatalytic, solar thermal and photoelectrochemical properties of aluminium-reduced black titania" Energy Environ. Sci., 2013, 6, 3007–3014.

34. C. Yang, Z. Wang, T. Lin, H. Yin, X. Lu¨, D. Wan, T. Xu, C. Zheng, J. Lin, F. Huang,

X. Xie and M. Jiang. “Core-shell nanostructured “black” rutile titania as excellent catalyst for hydrogen production enhanced by sulfur doping” J. Am. Chem. Soc., 2013, 135, 17831–17838.

35. G. Zhu, T. Lin, X. Lu, W. Zhao, C. Yang, Z. Wang, H. Yin, Z. Liu, F. Huang and J. Lin. “Black brookite titania with high solar absorption and excellent photocatalytic performance” J. Mater. Chem. A, 2013, 1, 9650–9653.
36. H. Yin, T. Q. Lin, C. Y. Yang, Z. Wang, G. L. Zhu, T. Xu, X. M. Xie, F. Q. Huang and M. H. Jiang. “Gray TiO_2 Nanowires Synthesized by Aluminum-Mediated Reduction and Their Excellent Photocatalytic Activity for Water Cleaning” Chem. – Eur. J., 2013, 19, 13313.
37. S. Tominaka, Y. Tsujimoto, Y. Matsushita and K. Yamaura. “Synthesis of nanostructured reduced titanium oxide: Crystal structure transformation maintaining nanomorphology” Angew. Chem., Int. Ed., 2011, 50, 7418–7421.
38. C. Barzan, E. Groppo, S. Bordiga and A. Zecchina. “Defect Sites in H_2-Reduced TiO_2 Convert Ethylene to High Density Polyethylene without Activator” ACS Catal., 2014, 4, 986–989.
39. L. Zeng, W. Song, M. Li, D. Zeng and C. Xie. “Catalytic oxidation of formaldehyde on surface of H-TiO_2/H, C-TiO_2 without light illumination at room temperature” Appl. Catal., B, 2014, 147, 490–498.
40. X. Lu, G. Wang, T. Zhai, M. Yu, J. Gan, Y. Tong and Y. Li. “Hydrogenated TiO_2 nanotube arrays for supercapacitors” Nano Lett., 2012, 12, 1690–1696.
41. C. Zhang, H. Yu, Y. Li, Y. Gao, Y. Zhao, W. Song, Z. Shao and B. Yi. “Supported Noble Metals on Hydrogen-Treated TiO_2 Nanotube Arrays as Highly Ordered Electrodes for Fuel Cells” ChemSusChem, 2013, 6, 659–666.
42. X.-Q. Zhang, J.-B. Chen, C.-W. Wang, A.-Z. Liao and X.-F. Su. “Low-temperature

liquid phase reduced TiO_2 nanotube arrays: synergy of morphology manipulation and oxygen vacancy doping for enhancement of field emission” Nanotechnology, 2015, 26, 175705.

43. T. Xia, C. Zhang, N. A. Oyler and X. Chen. “Hydrogenated TiO_2 nanocrystals: a novel microwave absorbing material” Adv. Mater., 2013, 25, 6905–6910.

44. T. Xia, Y. Cao, N. A. Oyler, J. Murowchick, L. Liu and X. Chen. “Strong Microwave Absorption of Hydrogenated Wide Bandgap Semiconductor Nanoparticles” ACS Appl. Mater. Interfaces, 2015, 7, 10407–10413.

45. F. Habashi, Handbook of Extractive Metallurgy, Wiley-VCH, Weinheim, Germany, 1997.

46. T. R. Gordon, M. Cargnello, T. Paik, F. Mangolini, R. T. Weber, P. Fornasiero and C. B. Murray. “Nonaqueous synthesis of TiO_2 nanocrystals using TiF_4 to engineer morphology, oxygen vacancy concentration, and photocatalytic activity” J. Am. Chem. Soc., 2012, 134, 6751–6761.

47. C. Zhang, S. Chen, L. E. Mo, Y. Huang, H. Tian, L. Hu, Z. Huo, S. Dai, F. Kong and X. Pan. “Charge recombination and band-edge shift in the dye-sensitized Mg^{2+}-doped TiO_2 solar cells” J. Phys. Chem. C, 2011, 115, 16418–16424.

48. B. Fang, J. H. Kim, M.-S. Kim and J.-S. Yu. “Hierarchical nanostructured carbons with meso–macroporosity: design, characterization, and applications” Acc. Chem. Res., 2013, 46, 1397–1406.

49. J. Yan, G. Wu, N. Guan, L. Li, Z. Li and X. Cao. “Understanding the effect of surface/bulk defects on the photocatalytic activity of TiO_2: anatase versus rutile” Phys. Chem. Chem. Phys., 2013, 15, 10978-10988.

50. Y. Xu, C. Zhang, L. Zhang, X Zhang, H. Yao and J. Shi. “Pd-catalyzed instant hydrogenation of TiO2 with enhanced photocatalytic performance” Energy Environ.

Sci., 2016, 9, 2410-2417

51. Z. Wu, W. Wang, Y. Cao, J. He, Q. Luo, W. A. Bhutto, S. Li and J. Kang. “A beyond near-infrared response in a wide-bandgap ZnO/ZnSe coaxial nanowire solar cell by pseudomorphic layers” J. Mater. Chem. A, 2014,2, 14571-14576

52. A. Fujishima and K. Honda. “Electrochemical Photolysis of Water at a Semiconductor Electrode” Nature,1972, 238, 37 - 38

요 약 문

가시광 이용하여 수소 생산하기 위한 산소결핍 블랙 타이타니아의 합성

본 연구는 광촉매로서 널리 알려져 있는 이산화 타이타늄 (TiO_2)에 인위적으로 결점을 생성함에 의해 광화학촉매적 성능을 향상시키는 방법을 제시하고 있다. 이산화 타이타늄은 넓은 밴드 갭으로 인해, 오직 자외선 영역의 빛에서만 광화학촉매적 역할을 하는 것으로 알려져 있다. 이를 해결하기 위해, 인위적으로 결점을 만들어 밴드 갭을 줄여 다양한 파장대의 빛을 활용하기 위한 연구가 되어왔다. 기존의 보고 된 방법들은, 밴드 갭을 줄여 빛 흡수 능력을 향상시키는데 성공했음에도, 많은 전자-정공 재결합 중심의 존재로 인해 충분히 광촉매활성능력을 향상시키는데 실패하였다. 이를 제어하기 위해서는 합성 방법이 결정적인 역할을 한다. 본 연구에서 마그네슘과 수소 가스를 동시에 이용하는 연구를 처음으로 시도하였으며, 결과적으로 적절한 이산화 타이타늄의 표면에 산소 결함, 수소 도핑, 표면 격자의 불규칙성 등의 결점을 형성하여 밴드 갭을 줄이며, 최적 양의 재결합 중심을 만들 수 있었다. 결과적으로 다양한 가시광선 및 적외선의 빛 또한 흡수하여 이용할 수 있었고, 광화학적 활성이 증가하였다. 특히, 물 분해를 이용한 수소 생성 반응에 우수한 활성을 보였다. 개발 된 재료 합성 방법을 통해 광촉매 뿐 아니라, 다른 여러 에너지 분야로의 응용이 기대된다.

Keywords: 광촉매, 물 분해, TiO_2, 밴드 갭, 산소 결함